Available online at www.sciencedirect.com
ScienceDirect
Journal of Power Sources 172 (2007) 768–774
JOURNAL OF POWER SOURCES
www.elsevier.com/locate/jpowsour

On the nanostructuring and catalytic promotion of intermediate temperature solid oxide fuel cell (IT-SOFC) cathodes

José M. Serra *, Hans-Peter Buchkremer

Forschungszentrum Jülich GmbH, Institute for Materials and Processes in Energy Systems, IEF-1, D-52425 Jülich, Germany

Received 16 October 2006; received in revised form 30 April 2007; accepted 13 May 2007
Available online 18 May 2007

Abstract

Solid oxide fuel cells (SOFCs) are highly efficient energy converters for both stationary and mobile purposes. However, their market introduction still demands the reduction of manufacture costs and one possible way to reach this goal is the decrease of the operating temperatures, which entails the improvement of the cathode electrocatalytic properties. An ideal cathode material may have mixed ionic and electronic conductivity as well as proper catalytic properties. Nanostructuring and catalytic promotion of mixed conducting perovskites (e.g. $La_{0.58}Sr_{0.4}Fe_{0.8}Co_{0.2}O_{3-\delta}$) seem to be promising approaches to overcoming cathode polarization problems and are briefly illustrated here. The preparation of nanostructured cathodes with relatively high surface area and enough thermal stability enables to improve the oxygen exchange rate and therefore the overall SOFC performance. A similar effect was obtained by catalytic promoting the perovskite surface, allowing decoupling the catalytic and ionic-transport properties in the cathode design. Noble metal incorporation may improve the reversibility of the reduction cycles involved in the oxygen reduction. Under the cathode oxidizing conditions, Pd seems to be partially dissolved in the perovskite structure and as a result very well dispersed.

Keywords: Fuel cell; Solid oxide fuel cell; SOFC; Perovskite; Electrocatalysts; Nanostructuring

1. Introduction

Solid oxide fuel cells (SOFCs) are promising candidates for high efficiency energy production in the near future. SOFCs allow transforming directly the chemical energy of a fuel into electrical energy producing as by-product a high-quality hot stream. This heat can readily be used for different applications, as for instance the co-generation by means of microturbines, increasing in turn the overall system efficiency. Fuel flexibility is one important advantage with respect to PEM fuel cells, since it is possible to feed, besides H_2, directly hydrocarbons into the cell anode. Especially interesting is the use of not only natural gas, diesel, (bio-)alcohols but also gasified coal or biomass [1–3]. In principle, SOFCs do not require external reforming, water–gas-shift and CO selective oxidation catalytic converters due to the anode internal reforming and the CO tolerance. Nevertheless, sulfur poisoning [4], coking and redox stability [5] at the anode are issues still to be enhanced. Indeed, the advantages of SOFC are as consequence of: (i) the high operating temperature (600–900 °C), allowing the use of non-precious metal electrocatalysts, heat recovery and the superior ionic conductivity of the different components; and (ii) the fact that the cell consists of assembled solid ceramic components. Nevertheless, the current SOFC technology suffers from two main drawbacks that must be overcome before up-scaling and launch to the market: (i) the high price of the produced kWh due to the manufacturing costs; and (ii) the high operating temperature (>750 °C), which increases the costs of construction materials and the starting-up time, shortens the operating life of the fuel cell stack, and therefore decreases the scope for domestic and vehicle power generation applications. As a consequence, there exists the need of improving the tolerance to direct hydrocarbon fueling with impurities and decreasing the operating temperature to 700–500 °C. Consequently, the catalytic performance and ionic conductivity of both electrodes have to be strongly improved at those intermediate temperatures. The current limita-

* Corresponding author. Present address: Instituto de Tecnología Química (UPV-CSIC), av. los Naranjos s/n, E-46022 Valencia, Spain.
Tel.: +34 963 877 819; fax: +34 963 877 809.
E-mail address: jsalfaro@itq.upv.es (J.M. Serra).

0378-7753/$ – see front matter © 2007 Elsevier B.V. All rights reserved.
doi:10.1016/j.jpowsour.2007.05.018

tion in the final performance of SOFCs operating with hydrogen or methane as fuel is sited in the electrochemical processes taking place in the air electrode (cathode), which entail different bulk and surface mechanisms [6–9]: (i) catalytic O_2 reduction, involving adsorption, dissociation, reduction and incorporation of the oxygen anion into the lattice; (ii) ionic transport through the porous perovskite electrode towards the electrolyte and (iii) ionic jump into the electrolyte lattice. Oxygen reduction step is currently [10] one of the biggest contributions to the total cell resistance and incremental improvements on the catalytic activity of the cathode would have a strong impact on the final cell power density.

It this work, two different approaches are pursued aiming to improve the overall performance of LSFC-based cathodes, i.e., by (i) increasing the surface area available for oxygen exchange, through the nanostructuring of the porous layer; and (ii) promoting the catalytic activity of the LSFC grain surface by impregnation/exchange with Pd and Rh. Several synthetic routes are tested to tailor the grain morphology and layer porosity. Moreover, the DC-electrochemical study is complemented by extensive fundamental material characterization (SEM, TEM, catalytic combustion test, N_2-sorption, XPS and XRD).

2. Experimental

Reference cathode LSM and LSFC materials were prepared by spray-drying process using nitrate salts as precursors. The obtained material was subsequently calcined at 900 °C for 3 h and ball-milled for 10 h. Materials with a slightly higher surface area were prepared by different complexation–gelation processes followed by final controlled pyrolysis (*Pechini* method). Mesoporous cathode materials were prepared following the procedure outlined elsewhere [11,12]. The corresponding metal nitrates were dissolved in a solution of ethanol and tri-block copolymer $HO(CH_2CH_2O)_{106}(CH_2CH(CH_3)O)_{70}(CH_2CH_2O)_{106}H$ (Pluronics F127, BASF) in a weight ratio perovskite to polymer of 1.4. The solution was gelled by evaporation and aged in a Petri-dish at 40 °C for a week. Finally, the obtained gel was pyrolized in air at 800 °C for 2 h using a 2 K min^{-1} heating rate. Phase purity was stated by XRD. Surface promoted samples were prepared by contacting the ball-milled powder ($d_{50} \sim 0.3$ μm) with a metal salt aqueous solution (Pd or Rh nitrates) under stirring at 80 °C for 5 h. Finally, the suspension was evaporated till dryness and the resulting solid calcined at 300 °C. The nominal metal content was 1 wt%.

SEM analysis was performed using a Zeiss Ultra55–INCAEnergy355 electron microscope and TEM analysis using a Philips CM200 microscope with LaB6 cathode. N_2 sorption was carried out on a Sorptomatic 1990 (Thermo Corp.) Pore size distribution analysis was computed following the Barret-Joyner-Halenda (BJH) method. XPS measurements were carried out in a XPS/AES spectrometer based on Physical Electronics components using dual Mg/Al X-ray tube (1253.6 eV/1486.6 eV).

Catalytic combustion of methane was carried out in a quartz fixed bed reactor with a 6 mm inner diameter. The bed consisted of 100 mg of the perovskite powder diluted in 2.5 ml of SiC ($d_{50} \sim 0.4$ mm). A mixture of Ar, CH_4 and O_2 in ratio 17/1/2 (v/v) and flow 400 ml min^{-1} was used as feed and the reaction products were analyzed online using a micro-GC (Varian CP-4900) equipped with Molsieve5A, PPQ and CP-Sil modules. Anode-supported cells with dimensions of 50 mm × 50 mm consisted of an anode substrate (averaged thickness of 1500 μm), an anode functional layer (thickness: 5–10 μm), and an electrolyte (thickness: 5–10 μm). The anode substrate, a porous composite consisting of NiO (Baker, USA) and 8 mol% yttria-stabilized zirconia (8YSZ, Unitec, UK), was formed by warm pressing using a so-called Coat-Mix® material and pre-sintered at 1230 °C [13]. Afterwards, the anode functional layer (NiO/8YSZ) and the electrolyte (8YSZ, Tosoh, Japan) were both deposited by vacuum slip casting and co-fired at 1400 °C, resulting in a gastight 8 μm-thick 8YSZ electrolyte. On top of this electrolyte layer, a $Ce_{0.8}Gd_{0.2}O_{2-\delta}$ layer (Treibacher, Austria; $d_{50} = 0.22$ μm), acting as a cation-diffusion barrier [14], was applied by screen printing (wet thickness: 34 μm and 40 mm × 40 mm geometry) and sintered at 1250 °C. The 40 mm × 40 mm cathode was composed of the corresponding LSFC material powder mixed with graphite and was applied by screen-printing (final thickness ~40 μm). The multilayer arrangement can be observed in

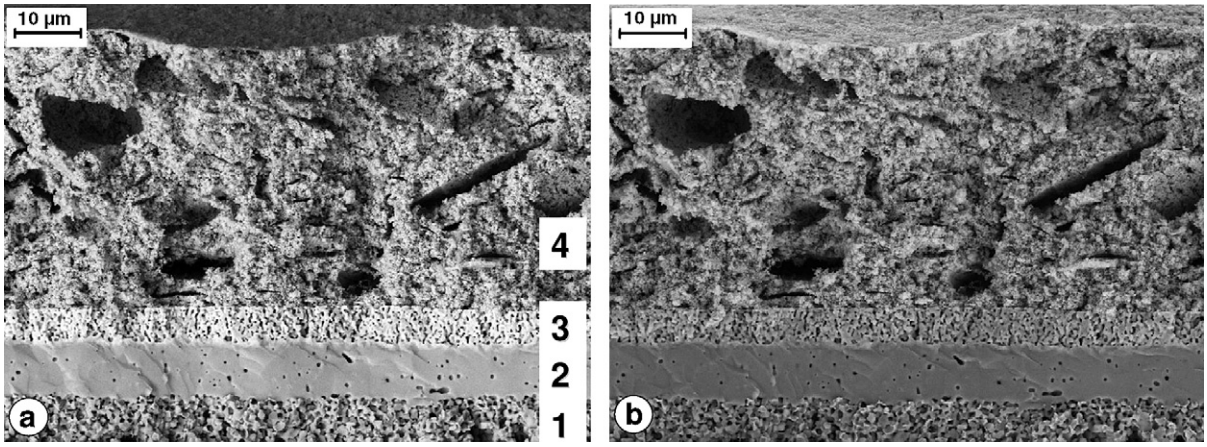

Fig. 1. Fracture cross-section of the mesoporous cathode cell after DC-electrochemical testing (a) BSE detector and (b) SE detector (both @EHT 15 kV, WD 9 mm). The multilayer assembly is clearly visible and the different layers correspond to: (1) fine-grained YSZ-Ni anode; (2) YSZ electrolyte; (3) CGO diffusion barrier, and (4) mesoporous LSFC cathode. Macropores are produced by removal of graphite platelets admixed in the screen-printing paste.

Table 1
Electrochemical performances of cells with different cathode materials: area specific resistance (ASR), power density and activation energy at 0.7 V

Material	Sintering temperature (°C)	ASR (mΩ cm^2)				Power density (W cm^{-2})				E_A (eV)
		800 °C	750 °C	700 °C	650 °C	800 °C	750 °C	700 °C	650 °C	
LSM spray-drying (reference)	1100	228	307	539	980	1.40	0.95	0.56	0.32	0.93
LSFC spray-drying	1080	176	213	258	470	1.81	1.44	1.01	0.61	0.63
Rh-LSFC complexation	900	169	204	261	468	1.83	1.46	1.03	0.6	0.66
LSFC complexation	900	188	247	350	651	1.64	1.17	0.81	0.44	0.79
Pd-LSFC complexation	900	155	193	247	468	1.99	1.47	1.05	0.59	0.70
LSFC-mesoporous	900	138	177	224	376	2.25	1.74	1.19	0.75	0.64
LSFC-mesoporous	800	230	274	381	626	1.21	1.02	0.74	0.46	0.66
LSFC spray-drying	800	170	259	411	608	1.99	1.49	0.93	0.53	0.82

the micrographs of Fig. 1. There can be seen the SEM analysis of an electrochemically tested fuel cell with a high surface cathode. Further details are available in Supplementary material. The addition of graphite (5%) aims to improve the sintering and form macropores, clearly visible in Fig. 1, for a fast oxygen transport. Indeed, it has been reported [15] that the addition of small amounts of graphite to LSCF paste improves the electrochemical properties of the cell when the cathode sintering temperature is as low as 800 °C. The cathodes sintered at temperatures higher than 900 °C do not contain graphite. DC-electrochemical measurements of cells were performed in an Al_2O_3 test housing placed inside of a furnace. Cell electrode connections to the electronic devices consisted of a Ni mesh at the anode side and a Pt mesh at the cathode side. Sealing of the gas compartment was obtained by a gold seal. The flow of wet (3%) hydrogen and air were both set at 1000 ml min^{-1}. The current–voltage characteristics were measured with increasing current load by a sequential step change of 62.5 mA cm^{-2} until the voltage dropped below 0.7 V.

3. Results and discussion

In principle, the simplest way to increase the O_2 reduction rate is by merely increasing the electrode surface area active for the charge-transfer processes. Mixed ionic-electronic conducting (MIEC) perovskites (e.g. $La_{0.58}Sr_{0.4}Fe_{0.8}Co_{0.2}O_{3-\delta}$-LSFC) are currently used as SOFC cathode material [16], typically prepared by spray-drying or sol–gel, and present a low surface area [17] in the range 1–5 m^2 g^{-1} after calcination at 900–1100 °C. These typical firing temperatures are required during the cell fabrication, in order to achieve a proper adhesion among the different ceramic layers and a lower resistance but leading to strong reduction of the electrode porosity.

Aiming to tailor the microstructure of the electrode materials [18], we prepared several cathode materials with the same nominal composition (LSFC) by spray-drying, citrate complexation and crystallization using tri-block copolymers. As a result, materials with different particle and pore morphology, and diverse surface areas were obtained. In Fig. 2 the particle size and

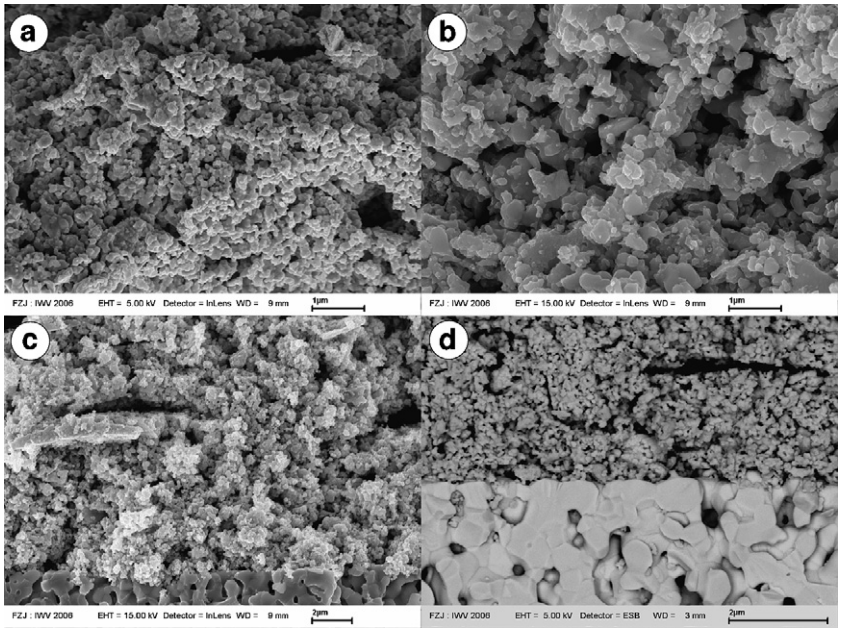

Fig. 2. Post-mortem microstructure analysis of evaluated cathodes. Fracture sections of cathodes with different textural properties: (a) mesoporous cathode and (b) complexation–gelation LSFC powder images recorded with InLens detector (SE) in a cathode area close to the electrolyte. Lower magnification pictures showing the Ce0.8Gd0.2O1.9 layer were recorded using (c) InLens (SE) and (d) ESB (BSE) detector, being possible to obtain compositional contrast. The cathodes were applied by screen printing, sintered at 900 °C and electrochemically tested in the range 650–900 °C.

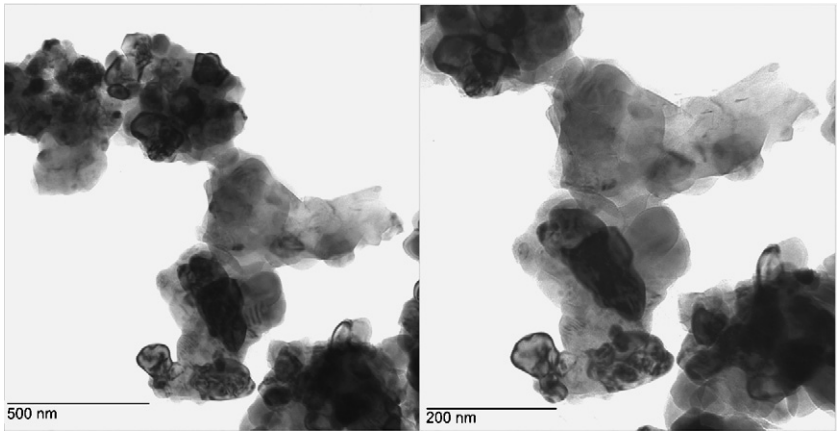

Fig. 3. TEM images of perovskite particles from a mesoporous cathode after cell DC-testing in the temperature range of 650–900 °C.

porosity of two cathodes synthesized by the last two routes are compared after firing and DC-electrochemical testing in the range 650–900 °C. The cathode obtained by using block copolymers exhibits a much lower particle size with pore diameter in the submicron range (mesoporosity) and therefore a higher surface area (BET 85 $m^2\,g^{-1}$ at 800 °C) than the other material (~12 $m^2\,g^{-1}$ at 800 °C). Moreover, this fine-grain structure is consolidated and well-attached to the underneath electrolyte composed of a screen-printed $Ce_{0.8}Gd_{0.2}O_{1.9}$ layer on an 8 μm-thick gastight $Zr_{0.85}Y_{0.15}O_2$ (8YSZ) layer. Fig. 1 shows two SEM images of the same cathode area, recorded with two detectors, i.e., SE and BSE detector. The different layers comprised in the cell are clearly recognizable and the different porosity of each. In addition, the BSE-detector allows distinguishing the changes in the composition, especially noticeable for the $Ce_{0.8}Gd_{0.2}O_{1.9}$ interlayer. The averaged size of the primary crystallites, agglomerated in larger particles and forming the cathode, is around 50 nm although an important fraction of crystallites smaller than 25 nm are observed by TEM and SEM in electrochemically tested cathodes (Fig. 3). The porosity and the relative high surface area are preserved despite the high firing temperature (900 °C). Fig. 4 presents the pore size distribution (BJH method) obtained with the N_2-adsorption isotherm. The electrochemical performance (DC polarization curves) of 16 cm^2-cells with these two cathodes materials plus a spray-dried $La_{0.65}Sr_{0.3}MnO_3$ (LSM) as reference cathode is presented in Fig. 5 and outlined in Table 1. This table summarizes the area

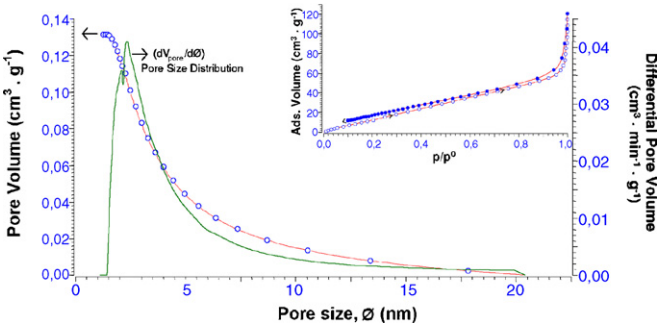

Fig. 4. Pore size distribution (BJH method) and N2 sorption isotherms of the mesoporous cathode sintered at 800 °C.

specific resistance (ASR) and power density at 0.7 V at different temperatures for cells with different cathode materials. The power density of the high surface area cathode is improved at every temperature from 650 to 800 °C with respect to the other two cells. The performance enhancement is especially visible at low temperatures, where the O_2 reduction is a major rate-limiting step. Considering that the surface area was increased by a factor of 5, a similar improvement would be expected on the catalytic activity. The higher catalytic activity was confirmed by measuring the combustion of CH_4 in a fixed bed reactor (Fig. 6). The evolution of CH_4 conversion and CO_2 yield at a contact time of 0.25 g l^{-1} min as a function of reaction temperature for both cathode materials corroborates the relation between surface area

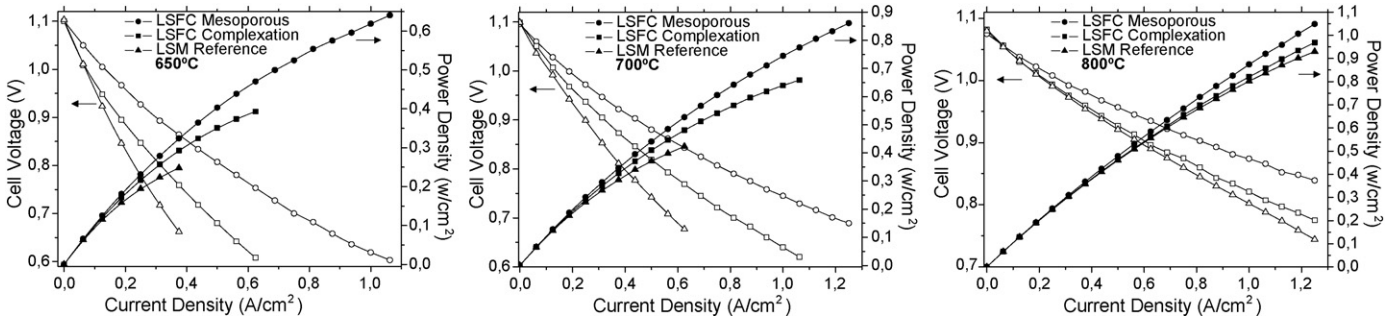

Fig. 5. Electrochemical performance (DC-curves) of 16 cm^2 fuel cells with different cathode materials: (1) mesoporous LSFC; (2) LSFC prepared by complexation–gelation; and (3) a reference LSM prepared by spray-drying. Air (11 min^{-1}) supplied to the cathode and wet H2 to the anode (11 min^{-1}). Open symbols for cell voltage (left axis) and solid symbols for power density (right axis).

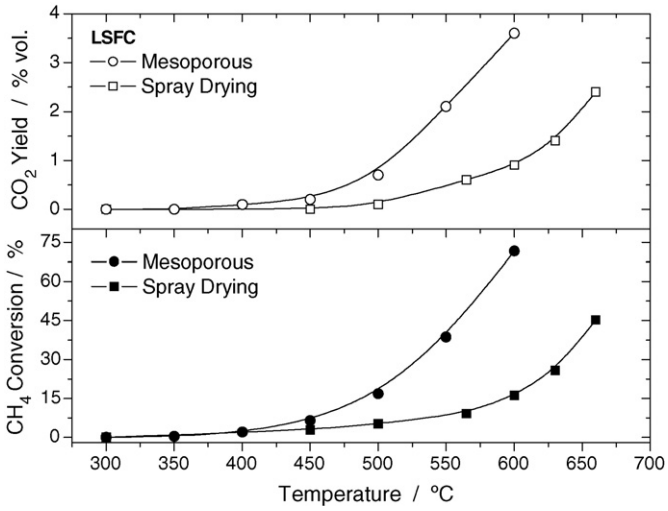

Fig. 6. Comparison of the catalytic combustion of methane of mesoporous and spray-dried LSFC materials.

and catalytic combustion. On the opposite, the relatively high fuel conversion obtained for both materials evidences the impossibility of using LSFC material as cathode for *single chamber fuel cells* [19], where selective O_2-reduction and poor fuel oxidation are mandatory on the cathode side. The mismatch between the surface area increase and the electrochemical improvement (cell resistance reduction of 40% at 700 °C) can be explained considering that (i) the improvement of the surface reaction rate on the cathode allows reducing the cathode polarization, but other serial resistances are still present on the electrolyte,[1] anode and interfaces between electrode and electrolyte; (ii) the nanostructuring of the porous cathode would affect other parameters, such as ionic transport through the cathode and charge-transfer process between cathode and electrolyte. The activation energy of the cell with the nanostructured cathode is 0.64 eV while the cells with low surface area present a higher value of 0.8 eV. This is an indication that after improvement of the cathode surface reactions, other electrochemical steps are governing the cell polarization in a higher extent.

When varying the perovskite synthesis method, an important factor to take into account is the sintering temperature for the cell fabrication. Indeed, a high temperature may destroy the fine surface structures composed by small crystallites but benefit the connectivity among particles, crucial to ensure the ionic current toward the electrolyte. Table 1 includes also the ASR and power density for cells sintered at different temperatures and with diverse cathode materials. Each material might have a different optimal thermal treatment and even a particular electrochemical activation process [20]. It can be seen that the mesoporous cathode fired at 900 °C performs even better than the spray-dried material sintered at its optimal temperature (1080 °C) [21]. Conversely, as the sintering temperature of the mesoporous cathode is reduced from 900 to 800 °C, the profit of the high surface area is missed, presumably due to low cathode compaction and poor connectivity with the electrolyte.

Apart from improving the surface area and pore system, another possibility for increasing the catalytic activity is the variation of the perovskite composition or at least the surface composition of the perovskite crystals. Rather than screening and optimizing the bulk composition of the SOFC cathodes, a more suited approach for increasing the cathode activity is the surface tailoring of a given perovskite composition with sufficient electronic and ionic conductivity. This catalytic promotion can be done by surface partial exchange of both A and B-cations of the most external planes of the perovskite crystallite, allowing the adjustment of adsorption and redox properties. Potential B-substituents are noble metals like Pd, Rh or Ag but the use of other single or multiple combinations of inexpensive metals could yield high reduction activities too. For this kind of studies, high-throughput screening technology may be a helpful method [22]. Another approach for cathode catalytic promotion is the impregnation of the porous perovskite with nanosized electrocatalyst (perovskites) particles produced by sol–gel techniques [23–25]. Two different effects can be argued to be responsible for the improvement of the promoted-cathode performances, i.e., the addition of intrinsically more active reduction sites (e.g. $SmCoO_{3-\delta}$) and the increase of the active surface area. Nevertheless, the introduction of precious or scarce metals as surface promoters may not raise the price of the SOFC manufacture, since these metals would be added in low amounts (∼1 wt.%) in the active cathode layer with a thickness 5–20 μm, that is, $\sim 130\ \mu g_{metal}\ cm_{cell}^{-2}$.

This approach is illustrated in Fig. 7, which presents the electrochemical performance of cells with a pristine LSFC cathode prepared by citrate complexation, and two cells with surface-promoted LSFC composed of the same starting LSFC material impregnated with Rh (1%) and Pd (1%). The addition of Pd improves significantly the performance in the whole range of temperatures while Rh improves as well the performance at lower temperatures but in a lower degree than Pd. Both metals are very finely dispersed on the perovskite surface and the particles are not detectable by TEM ($\emptyset < 5$ nm), as shown in Fig. 8. Post-mortem XPS analysis of the Pd-promoted-cathode surface electrochemically tested at 900 °C showed that only around 20% of the Pd is present as metal (at room temperature) and the rest shows an oxidation state related to PdO_3 species [26,27] (see Table 2), presumably incorporated in the perovskite in the B-position (hexacoordinated). It has been already observed the Pd-solubility in ferrites [28,29], catalyzing NO reduction with C_3H_6. This similar approach was successfully applied [30] in the development of self-regenerative automotive emission catalysts ($LaFe_{0.57}Co_{0.28}Pd_{0.05}O_{3-\delta}$) and it was stated by EXAFS that Pd occupies B-site perovskite position in oxidized state [31]. Moreover, it was observed the reversible segregation of Pd nanoparticles (partially alloyed with Co) after exposure at reducing conditions and subsequent reincorporation into the perovskite structure under oxidizing conditions. In the case of our Pd-promoted-cathode, the polarization caused by gaseous transport limitation at very high current densities might lead to the surface-localized decrease of the oxygen partial pressure, which

[1] For instance, the YSZ-electrolyte ASR of this cell is ca. 50 mΩ at 700 °C, which represents approximately 25% of the total cell ASR.

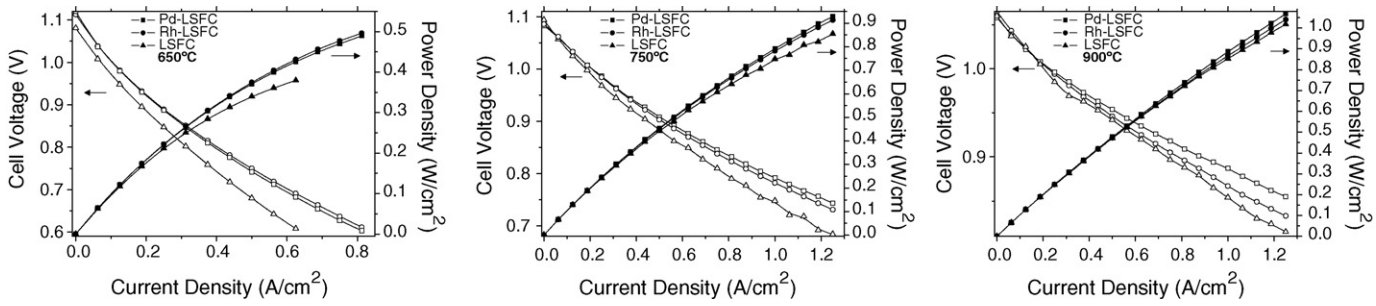

Fig. 7. Electrochemical performance (DC-curves) of 16 cm^2 fuel cells with different cathode materials: pristine complexation–gelation LSFC, Pd- and Rh-promoted LSFC. Open symbols for cell voltage (left axis) and solid symbols for power density (right axis).

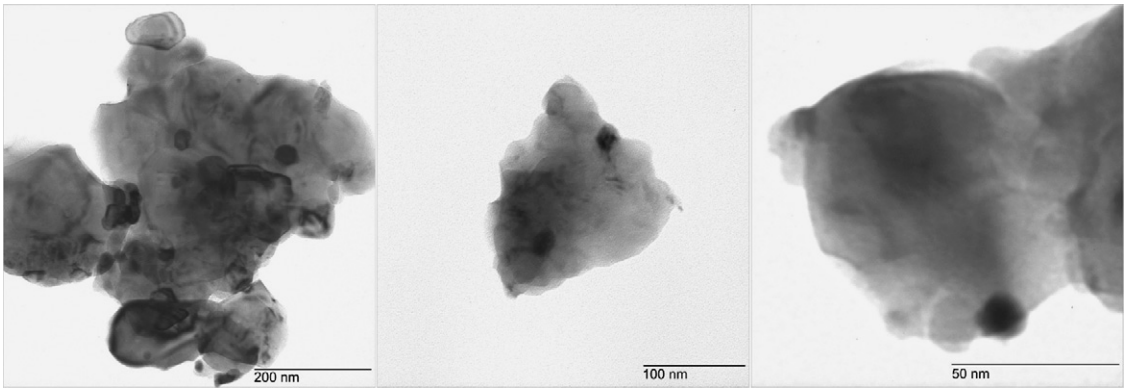

Fig. 8. TEM image of Pd-promoted LSFC cathode particles from a cell tested at 900 °C.

Table 2
Atomic abundance relative to the CH_2 (contamination) binding energy at 285.0 eV and surface distribution in % (relative error = ±15%)

Ox-state (bond)	LSFC unreacted cathode calcined at 800 °C BE (eV)/%	Pd-LSFC electrochemically tested at 900 °C BE (eV)/%
La		
$XLaO_3$	833.1/2.1	833.3/1.3
La_2O_3	834.3/2.1	834.4/1.9
Co		
Co	777.3/0.1	777.4/0.1
Co_2O_3	779.6/1.8	780.0/2.1
CoO	781.1/1.3	781.4/1.4
Sr		
$SrXO_3$	131.9/2.8	132.1/7.4
$SrYO_4$	133.4/4.8	133.9/3.6
SrO	135.8/0.9	
Fe		
FeO	709.1/1.6	709.4/2.0
Fe_2O_3	710.3/5.0	710.5/6.1
Pd		
Pd	–	335.6/0.02
PdO_3		337.5/0.08
O		
MeO_x	528.4/10.8	528.7/16.0
MeO_x	529.3/9.8	529.6/17.8
MeO_x, Kont.	531.2/25.9	531.6/23.7
Ads. H_2O	533.6/5.5	533.1/2.9
C		
CH_2	285.0/17.7	285.0/7.5
COC, COH	286.2/5.7	286.1/1.6
COOH	288.8/2.1	288.8/2.7
CO_3^{2-}		290.6/0.4

Note: Binding energy (BE) references available in http://srdata.nist.gov/xps/Elm_in_comp.htm. Measurement performed at room temperature

could lead to the (reversible) segregation of Pd nanoparticles on the perovskite surface.

With respect to the Pd role in the cathode reaction mechanism, Pd would improve the redox cycles of Fe and Co, active species on the crystallite surface, and enable the reaction with a smaller energy barrier, leading to the reduction of the adsorbed oxygen at lower temperatures. A tentative mechanism would involve the adsorption of molecular oxygen (α-O_2) and subsequent dissociation followed by the filling of the surface oxygen vacancies ($V_O^{\bullet\bullet}$) by molecular/atomic oxygen. At this point, charge-transfer takes place and oxygen is reduced with the formation of electronic holes ($h^{\bullet}$), related to oxidized Fe, Co cations, and finally the O^{2-} diffusion to bulk vacancies in the direction of the electrolyte. The regeneration of the oxidized cations with electrons from the interconnect and the incorporation in the oxygen vacancy [32] may be then promoted by lattice Pd and/or adjacent metallic Pd.

This kind of catalytic promotion is notably more visible for MIEC cathode materials, since the whole electrode surface area is participating in oxygen exchange process, in contrast with LSM-based electrodes [33,34] (pure electronic conductor) where the exchange is limited to the three-phase-boundary and the Pd dispersion was very poor, due probably to low solubility in the perovskite structure.

4. Conclusions

In summary, the present results suggest that the combination of nanostructuring and surface catalytic promotion of SOFCs cathodes would allow overcoming polarization problems when decreasing the cell operating temperature. The preparation of relatively high surface area cathodes with enough thermal stability enables to improve the oxygen exchange rate and therefore the overall SOFC performance. A similar effect was obtained by catalytic promoting the perovskite surface, allowing decoupling the catalytic and ionic-transport properties in the cathode design. Pd incorporation may improve the reversibility of the reduction cycles involved in the oxygen reduction, restoring the Fe and Co oxidation state after O^{2-} incorporation in bulk oxygen vacancies. Under the cathode oxidizing conditions, Pd seems to be partially dissolved in the perovskite structure and as a result very well dispersed.

Acknowledgements

J.M.S. is indebted to Fundación Ramón Areces for institutional and financial support. The authors thank J. Mertens and M. Kampel for the preparation of SOFC supports, D. Sebold for SEM analysis, P. Lersch for XRD measurements, A. Besmehn and U. Breuer (Zentralabteilung für Chemische Analysen) for XPS analysis, V.A.C. Haanappel for electrochemical testing and H.J. Penkalla for TEM analysis.

Appendix A. Supplementary data

Supplementary data associated with this article can be found, in the online version, at doi:10.1016/j.jpowsour.2007.05.018.

References

[1] A.J. Ragauskas, et al., Science 311 (2006) 484–489.
[2] G.W. Huber, S. Iborra, A. Corma, Chem. Rev. (2006) 4044–4098.
[3] S. McIntosh, R. Gorte, Chem. Rev. 104 (2004) 4845–4865.
[4] P.J. de Wild, R.G. Nyqvist, F.A. de Bruijn, E.R. Stobbe, J. Power Sources 156 (2) (2006) 995–1004.
[5] Q.X. Fu, F. Tietz, P. Lersch, D. Stöver, Solid State Ionics 177 (2006) 1059–1069.
[6] S.B. Adler, Chem. Rev. 104 (2004) 4791.
[7] S.B. Adler, X.Y. Chen, J.R. Wilson, J. Catal. 245 (2007) 91–109.
[8] E. Ivers-Tiffee, A. Weber, H. Schichlein, in: W. Vielstich, A. Lamm, H.A. Gasteiger (Eds.), Handbook of Fuel Cells, vol. 2, John Wiley & Sons Ltd., Chichester, England, 2003, pp. 587–600 (Hrsg).
[9] P.J. Gellings, H.J.M. Bouwmeester, Catal. Today 58 (2000) 1–53.
[10] F.S. Baumann, J. Fleig, H.-U. Habermeier, J. Maier, Solid State Ionics 177 (2006) 1071–1081.
[11] P. Yang, D. Zhao, D.I. Margolese, B.F. Chmelka, G.D. Stucky, Nature 396 (1998) 152–155.
[12] J.M. Serra, S. Uhlenbruck, W.A. Meulenberg, H.P. Buchkremer, D. Stöver, Top. Catal. 40 (1–4) (2006) 123–131.
[13] D. Stöver, H.P. Buchkremer, F. Tietz, N.H. Menzler, in: J. Huijsmans (Ed.), Proceedings of the Fifth European Solid Oxide Fuel Cell Forum, Lucerne, Switzerland, 1–5 July 2002, European Fuel Cell Forum, Oberrohrdorf, Switzerland, 2002, pp. 1–9.
[14] W.G. Wang, M. Mogensen, Solid State Ionics 176 (2005) 457–462.
[15] R.J. Gorte, J.M. Vohs, US Patent 6,958,196 to Pennsylvania University, 2005.
[16] H.L. Tuller, J. Schoonman, I. Riess (Eds.), Oxygen Ion and Mixed Conductors and their Technological Applications, Kluwer Academic, Dordrecht, The Netherlands, 2000.
[17] H. Hujii, N. Mizuno, M. Misono, Chem. Lett. (1987) 2147–2150.
[18] A. Rainer, F. Basoli, S. Licoccia, E. Traversa, J. Am. Ceram. Soc. 89 (2006) 1795–1800.
[19] M. Shao, S.M. Haile, Nature 431 (2004) 170–173.
[20] S. Koch, M. Mogensen, P.V. Hendriksen, B. Dekker, B. Rietveld, Fuel Cells 6 (2006) 117–122.
[21] A. Mai, V.A.C. Haanappel, S. Uhlenbruck, F. Tietz, D. Stöver, Solid State Ionics 176 (2005) 1341–1350.
[22] A. Corma, J.M. Serra, Catal. Today 107 (2005) 3–11.
[23] T.Z. Sholklapper, C. Lu, C.P. Jacobson, S.J. Visco, L.C. De Jonghe, Electrochem. Solid-State Lett. 9 (2006) A376–A378.
[24] C. Peters, B. Rüger, U. Guntow, L. Dieterle, A. Weber, E. Ivers-Tiffée, Presented in the E-MRS (Solid State Ionics Symposium), Nice, France, 29 May–2 June, 2006.
[25] A. Weidenkaff, Adv. Eng. Mater. 6 (2006) 709–714.
[26] J.M. Tura, P. Regull, L. Victori, M. Dolors de Castellar, Surf. Interface Anal. 11 (1988) 447.
[27] J. Li, U.G. Singh, J.W. Bennett, K. Page, J.C. Weaver, J.-P. Zhang, T. Proffen, A.M. Rappe, S. Scott, R. Seshadri, Chem. Mater. 19 (2007) 1418–1426.
[28] R. Zhang, A. Villanueva, H. Alamdari, S. Kaliaguine, J. Catal. 237 (2006) 368–380.
[29] R. Zhang, H. Alamdari, S. Kaliaguine, J. Catal. 242 (2006) 241–253.
[30] H. Tanaka, Catal. Surv. Asia 9 (2005) 63–74.
[31] Y. Nishihata, J. Mizuki, T. Akao, H. Tanaka, M. Uenishi, M. Kimura, T. Okamoto, N. Hamada, Nature 418 (2002) 164–167.
[32] R. Merkle, J. Maier, J.H.M. Boumeester, Angew. Chem. 116 (2004) 5179–5183.
[33] V.A.C. Haanappel, D. Rutenbeck, A. Mai, S. Uhlenbruck, D. Sebold, H. Wesemeyer, B. Röwekamp, C. Tropartz, F. Tietz, J. Power Sources 130 (2004) 119–128.
[34] R.A. De Souza, Phys. Chem. Chem. Phys. 8 (2006) 890–897.